Contrib Mineral Petrol (2009) 157:411–427
DOI 10.1007/s00410-008-0342-9

ORIGINAL PAPER

Tourmaline geochemistry and δ^{11}B variations as a guide to fluid–rock interaction in the Habachtal emerald deposit, Tauern Window, Austria

Robert B. Trumbull · Marc-Sebastian Krienitz · Günter Grundmann · Michael Wiedenbeck

Received: 25 April 2008 / Accepted: 29 August 2008 / Published online: 18 September 2008

Abstract Tourmalines from the Habachtal emerald deposit in the Eastern Alps formed together with emerald in a ductile shear zone during blackwall metasomatism between pelitic country rocks and a serpentinite body. Electron microprobe and secondary ion mass spectrometric (SIMS) analyses provide a record of chemical and B-isotope variations in tourmalines which represent an idealized profile from metapelites into the blackwall sequence of biotite and chlorite schists. Tourmaline is intermediate schorl-dravite in the country rock and become increasingly dravitic in the blackwall zones, while F and Cr contents increase and Al drops. Metasomatic tourmaline from blackwall zones is typically zoned optically and chemically, with rim compositions rich in Mg, Ti, Ca and F compared with the cores. The total range in δ^{11}B values is −13.8 to −5.1‰ and the within-sample variations are typically 3–5‰. Both of these ranges are beyond the reach of closed-system fractionation at the estimated 500–550°C conditions of formation, and at least two boron components with contrasting isotopic composition are indicated. A key observation from tourmaline core analyses is a systematic shift in δ^{11}B from the country rock (−14 to −10‰) to the inner blackwall zones (−9 to −5‰). We suggest that two separate fluids were channeled and partially mixed in the Habachtal shear zone during blackwall alteration and tourmaline-emerald mineralization. A regional metamorphic fluid carried isotopically light boron as observed in the metapelite country rocks. The other fluid is derived from the serpentinite association and has isotopically heavier boron typical for MORB or altered oceanic crust.

Keywords SIMS · B-isotopes · Tourmaline · Sector zoning · Blackwall alteration · Eastern Alps

Communicated by J. Hoefs.

Electronic supplementary material The online version of this article (doi:10.1007/s00410-008-0342-9) contains supplementary material, which is available to authorized users.

R. B. Trumbull (✉) · M.-S. Krienitz · M. Wiedenbeck
GFZ German Research Centre for Geosciences, Telegrafenberg, 14473 Potsdam, Germany
e-mail: bobby@gfz-potsdam.de

G. Grundmann
Technische Universität München, Arcistrasse 21, 80333 München, Germany

Introduction

Ultramafic rocks caught up in collisional orogens like the Himalayan-Alpine chain commonly end up as dismembered bodies of serpentinite strung out along regional shear zones. The combination of intense deformation and fluid channeling in these zones, along with the strong geochemical contrast between serpentinite and crustal wallrocks can produce a particularly vivid form of fluid–rock interaction known as blackwall zoning (Phillips and Hess 1936; Curtis and Brown 1969; Bucher et al. 2005). Excellent examples of this are exposed in the Tauern Window of the Eastern Alps, where the additional factors of regional metamorphism and ductile deformation led to the development of spectacular metasomatic rock assemblages in which the processes of mid-crustal shearing and fluid–rock interaction are well preserved (Morteani 1974; Okrusch et al. 1981; Grundmann and Morteani 1982; Barnes et al. 2004). Blackwall zoning has also been described in subduction zone melange associations (e.g., Bebout and Barton 2002; King et al. 2003; Altherr et al. 2004; Marschall et al. 2006). The latter two examples are

of particular relevance to the present study because tourmaline formed in the blackwall zones and its chemical and B-isotopic compositions were used to shed light on the nature of subduction zone fluids.

The subject of this paper is a well-studied example of blackwall zoning in the Habachtal locality in the eastern Tauern Window, which has the distinction of hosting one of Europe's few important emerald deposits. Habachtal emeralds were systematically mined from underground workings from the early 1860s until 1939, with a peak production of 68,000 carats in 1903 (Grundmann 1991). Detailed microtextural and geochemical studies of the emeralds and their host rocks (Grundmann and Morteani 1982, 1989) established that emerald formation was related to blackwall metasomatism in a regional shear zone that justaposed serpentinite and aluminous country rocks. Tourmaline is part of the same mineral paragenesis as emerald in the blackwall zones and it also occurs in the garnet–mica schists from outside the shear zone. The blackwall tourmalines are optically zoned and show distinctive changes in the abundance and internal fabric of mineral inclusions from core-to-rim that are also found in emerald porphyroblasts in the same rocks. Tourmaline is more widespread than emerald in these rocks and its large chemical variability makes it a potentially valuable monitor of fluid–rock interaction in the blackwall zones. The present study sets out to document the chemical and B-isotopic variations of tourmalines from an idealized profile from the country rocks into the blackwall zones. Although the Habachtal metasomatic rocks and similar units from the Tauern Window have been the subject of many geochemical and petrologic studies in the past, this is the first investigation of tourmaline compositions.

Geological setting

The Habachtal emerald deposit is situated in the Tauern Window of the Eastern Alps, where late Paleozoic (Variscan) Penninic units from beneath the Austroalpine nappes are exposed (Fig. 1a). The deposit is hosed in a regional shear zone that developed along the contact between granodiorite orthogneisses of the the "Zentralgneis" massif (with U-Pb zircon age of 314 ± 7 Ma, Cliff 1981) and a variegated metamorphic sequence called the Habach Group (metapelites and metavolcanics, with local serpentinite bodies). Structurally, the Habach Group is part of the lower schist cover, which is interpreted as a nappe emplaced above the Zentralgneis during the Alpine orogeny (Sm–Nd garnet ages of 30 ± 1 Ma, Christensen et al. 1994). Cutting across the Zentralgneis massif in the Tauern Window is the Greiner zone (Fig. 1a), a ductile shear zone along which the orthogneiss country rocks are locally transformed to biotite and chlorite schists. Several small bodies of serpentinite also occur along the Greiner zone (Melcher et al. 2002) and these display the same phenomena of blackwall contact metasomatism against the felsic country rocks as at Habachtal, but without emerald mineralization. The deformation and metasomatism along the Greiner zone were studied in detail by Barnes et al. (2004). They concluded from chemical, stable isotope (O, H) and mineralogic data that the metasomatizing fluids in the Greiner zone were derived from serpentinite dehydration. The serpentinites are part of the Penninic units and predate Alpine metamorphism, whereas the dehydration event and shear deformation are related to the Alpine event (Barnes et al. 2004). Many of the features described by Barnes et al. (2004) from the western Tauern Window are also found in the Habachtal locality, which lies along strike of the Greiner shear zone to the east (Fig. 1a). Textural and petrographic evidence combined with mineral thermobarometry, O-isotope thermometry and fluid inclusion analysis from rocks of the Habach Group by Hoernes and Friedrichsen (1974), Grundmann (1989) and Nwe and Grundmann (1990) documented both a pre-Alpine and an Alpine tectono-metamorphic event. According to these studies, the peak P–T conditions of the pre-Alpine event were about 300 MPa and 450°C, whereas the Alpine event reached higher grade (450–600 MPa and 500–550°C) and partially overprinted the earlier assemblages.

The lithologic sequence of blackwall alteration zones at Habachtal comprises the following rock types, progressing from the serpentinite body to the pelitic schists of the Habach Group to the SE (Fig. 1b): antigorite–serpentinite, talc schist, talc–actinolite schist, chlorite schist, biotite schist, biotite–albite schist, and garnet–mica schist. Note that this sequence is idealized from several profiles across the deposit, and in reality the intense shear deformation has produced a tectonic mélange with extreme local variations in thickness of the zones and intensity of metasomatism. Based on whole-rock geochemical profiles across the blackwall zones, Grundmann (1983) and Grundmann and Morteani (1989) placed the original contact of the serpentinite and wallrocks at the present boundary between the chlorite zone and the talc–actinolite zone. Blackwall alteration is developed on both sides of the serpentinite body, (Fig. 1b), but beryl and tourmaline occur only on the SE side of the profile, where the country rocks are pelitic schists of the Habach Group.

Detailed microtextural studies of tourmaline, emerald and plagioclase porphyroblasts by Morteani and Grundmann (1977), Grundmann (1983, 1989), Grundmann and Morteani (1982, 1989) have established a deformation-crystallization history for the Habachtal rocks, summarized in Fig. 3, all of which is related to the Alpine event. An early, syn-deformational prograde phase is recorded

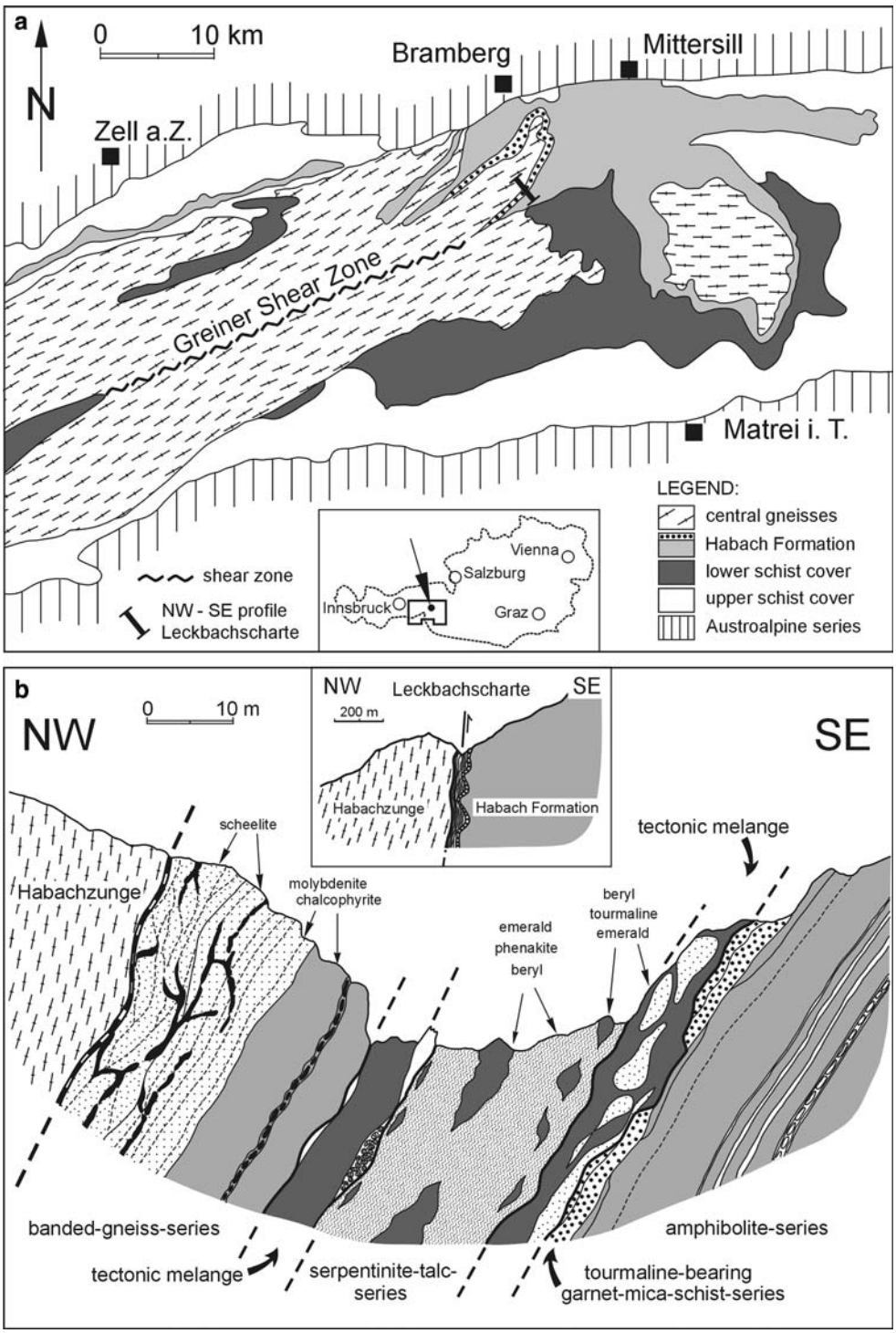

Fig. 1 **a** Location map of the Tauern Window in the eastern Alps, Austria, showing the important tectonic units: central gneisses, Lower Schist Cover and Upper Schist Cover. The Habach Group which hosts the deposit is part of the Lower Schist Cover. Also shown with the "s" pattern is the ductile Greiner shear zone, which cuts through the central gneisses and hosts several serpentinite bodies along it. The Habachtal deposit (*profile symbol*) occurs along strike of the Greiner shear zone at the tectonic contact between the central gneisses (Habachzunge) and the Lower Schist Cover. **b** Lithologic cross section of the Habachtal deposit after Grundmann and Morteani (1989). On the W-side of the profile is the tectonic contact between the granitic orthogneisses of the Habachzunge and banded gneisses and amphibolites of the Habach Group. Metasomatic blackwall zones are developed in highly sheared melange zones surrounding tectonic lenses of the "serpentinite-talc series". The emerald mineralization and the occurrence of tourmaline is confined to the eastern side of the profile in tectonic melange at contacts with the metapelitic unit in the Habach Group (garnet–mica schist series)

by inclusion-rich and locally rotated crystal cores. This was followed by at least one higher-temperature and largely post-deformational phase which is marked in the crystals by inclusion-free rims. Barnes et al. (2004), in their study of metasomatic rocks from the Greiner zone west of Habachtal, also concluded that the peak metamorphic conditions followed the main deformation event. Also associated with the prograde, post-deformational phase at Habachtal was the formation of massive quartz veins up to 2 m thick and 200 m in outcrop extent in the talc schist on the NW side of the profile (Fig. 1b). Finally, a retrograde metamorphic phase in these rocks involved brittle deformation with formation of albite, chlorite and biotite.

Information about the fluid composition and conditions of emerald formation comes from a detailed fluid inclusion study by Nwe and Grundmann (1990), who distinguished an early and late generation of primary inclusions based on their position in zoned emerald porphyroblasts. These two fluid generations differ significantly in terms of bulk density and the proportion of CO_2 ($X_{CO_2} < 4$ vol% in the early generation and up to 11 vol% in later fluids). The relative increase in CO_2 in later fluids was attributed to consumption of H_2O by prograde hydration reactions in the blackwall alteration process (see "Discussion" below). Microthermometry data allowed construction of a temperature–pressure-time path which demonstrated that mineral growth was prograde, with formation of the crystal rims at temperatures corresponding to the peak Alpine metamorphism (500–550°C).

Petrography of the tourmaline samples

The distribution of samples selected for this study is shown on an idealized sketch of the blackwall sequence in Fig. 2. We distinguish three groups of samples, representing the main host lithologies from unaltered country rocks into the emerald-bearing blackwall alteration zones, as follows:

1. The country rock unit, of garnet–mica schist with lenses of plagioclase–biotite gneiss, which forms a layer up to 2 m thick within the Habach Group. It contains tourmaline and quartz-rich stringers and lenses up to 3 cm thick which are parallel to foliation and often finely folded. The tourmaline in this unit generally forms dark brown to black isolated grains or fine grained, massive aggregates of up to 2 cm in size. It is represented in this study by sample 103-b.

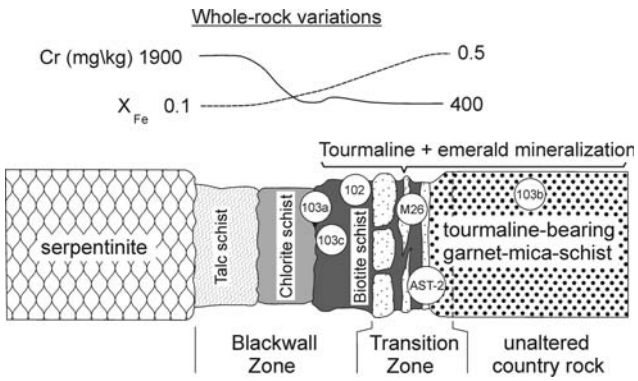

Fig. 2 Schematic sketch of the blackwall zones between serpentinite and garnet–mica schist, with the location of samples used from this study. The chemical profiles shown for Cr (mg/kg) and X_{Fe} represent whole-rock compositional trends given by Grundmann (1983)

2. A transitional zone between unaltered garnet–mica schist and the blackwall rocks. The transition zone rocks sampled for this study are white to light gray albite–muscovite schist (sample M26) and light gray to dark brown biotite–muscovite schist (AST-2), which form irregular medium to very fine-grained layers and boudinaged lenses between the garnet-mica schist and the blackwall zones. The tourmaline in these rocks typically forms dark brown to black, fine-grained aggregates up to 2 cm in size, which are parallel to the main foliation. Isolated columnar or acicular crystals also occur and clumps of these reach up to 4 cm in length.
3. The blackwall alteration zones, consisting of biotite- and chlorite-schists which form irregular lenses and layers up to 1 m in thickness. The tourmaline in these samples is dark brown to black and generally forms medium to fine grained, isolated, needle-like crystals and crystal groups of up to 5 cm in length which are homogenously distributed without distinct preferred orientation. Our blackwall samples represent biotite schist (103-c), biotite–chlorite schist (sample 102) and chlorite schist (103-a). Sample 102 is noteworthy because tourmaline is found as inclusions in emerald porphyroblasts.

Establishing the relationship of tourmaline growth to the sequence of deformation, metamorphism and blackwall alteration is vital for interpreting the geochemical results so it is useful to summarize the textural evidence here. As mentioned above, the metamorphic rocks at Habachtal underwent two main events of regional metamorphism (Variscan and Alpine). The ductile shearing and metasomatism which produced blackwall alteration and mineralization were related to the Alpine event.

Tourmaline from garnet–mica schist outside the mineralized shear zone typically forms crystal aggregates of light to dark brown, euhedral to anhedral crystals. Individual grain sizes range between 0.01 and 0.1 mm in diameter. Color zoning is weak and there are only few mineral inclusions. The mineral assemblage with tourmaline includes quartz, biotite, plagioclase, titanite, garnet, ilmenite, pyrite, pyrrhotite, apatite, zircon and graphite. Locally, larger tourmaline grains of this type show two phases of growth where the rocks have been affected by Alpine-age deformation. The clearest examples of this are where large, brown tourmaline grains are fractured by the Alpine deformation and show overgrowths and crack-fillings of lighter brown-blue tourmaline (Fig. 4a, b). In other cases, the younger tourmaline is recognized as fine-grained polygonal aggregates that formed at the expense of older tourmaline due to strain-induced grain boundary migration and size reduction (Fig. 4c, d).

A very different variety of tourmaline is typical for the blackwall alteration zones (biotite schist and chlorite schist). In these rocks, tourmaline occurs as isolated, non-oriented, euhedral porphyroblasts, which are commonly strongly zoned optically and contain abundant mineral inclusions, particularly in the cores. Typical grain size range between 0.1 and 1 mm in diameter and 1 and 10 mm in length. This variety occurs alongside variety one in the transitional sample AST-2 whereas it is the only one found in M-26 and in the blackwall samples. The detailed study of microtextures in tourmaline, emerald and plagioclase porphyroblasts from the Habachtal blackwall rocks by Grundmann (1983) found that all three phases show the same sequence of crystal growth and internal fabric development which indicate the main phase of growth (inclusion-rich cores) during the Alpine deformation and a later, more static growth of crystal rims. A synoptic sketch is shown in Fig. 3 and examples from the samples in this study are shown in Fig. 4e, f. The color zoning in blackwall tourmalines is striking and commonly complex, with up to 6 more or less sharply separate zones distinguished by yellow–green, blue–green, olive–green, light-brown, dark-brown and light-blue hues. A special feature of tourmalines from the biotite and chlorite schists is the development of hourglass sector zoning (Fig. 4g, h). Sector zoning in tourmaline has recently attracted attention (van Hinsberg et al. 2006; van Hinsberg and Marschall 2007; van Hinsberg and Schumacher 2007) and more details of the Habachtal occurrence are given below.

Analytical methods

Electron microprobe analysis

Tourmaline compositions were determined on polished and carbon-coated 2.5 cm round thin sections by wavelength-dispersive electron microprobe analyses at the GFZ Potsdam. The CAMECA SX-100 microprobe was operated at 15 kV accelerating voltage and 20nA beam current. Natural oxide and silicate mineral reference materials were used for calibration and data reduction employed the method of Pouchou and Pichoir (1984). Our procedure for microprobe analysis was to routinely analyze two or more points from the core and rim portions of optically zoned grains to check for chemical variations. Tourmaline structural formulae were calculated assuming stoichiometric 3.0 B per formula unit and by normalizing to 15 cations in the tetrahedral and octahedral sites (T + Z + Y) according to the suggestion of Henry and Dutrow (1996). The structural formulae are approximate to the extent that our chemical analyses are not complete; we did not determine B, H_2O, ferrous/ferric iron ratio, and minor elements such as Li and Zn, which may be present at sub-wt.% level. X-ray element maps illustrating the hourglass sector zoning of tourmaline in sample 103a (see Fig. 4h) were collected with the JEOL Hyperprobe JXA-8500F electron microprobe at the GFZ Potsdam, whose field-emission electron gun permits an extremely small beam diameter at the sample surface (ca. 80 nm for the 15 kV accelerating voltage and 50 nA beam current used here).

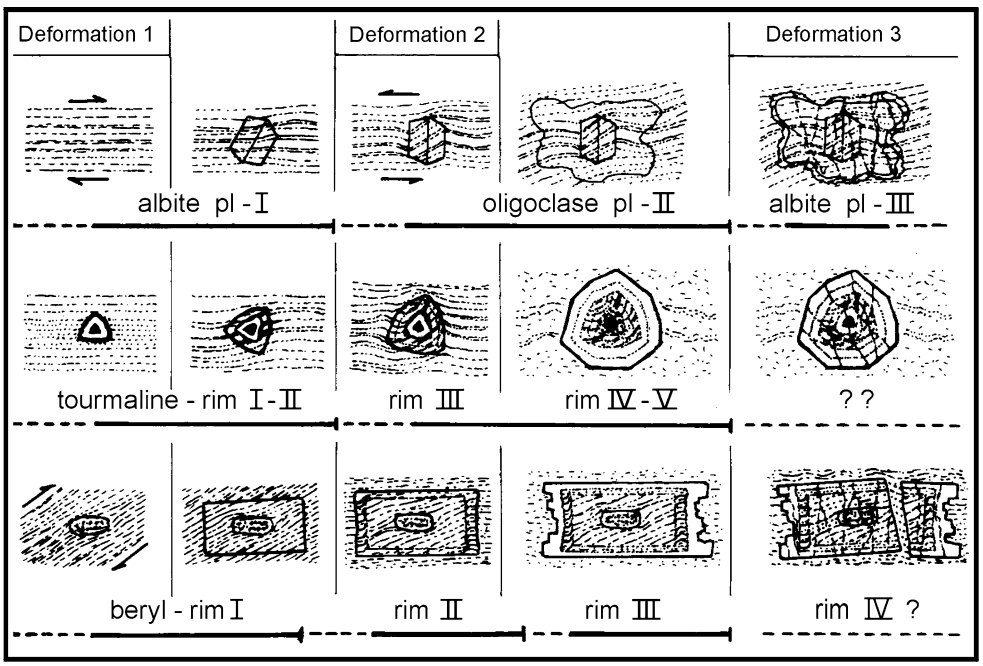

Fig. 3 Metamorphic crystallization/deformation diagram for plagioclase, tourmaline and beryl porphyroblasts in the blackwall-zone rocks in the Habachtal deposit, compiled from published structural, petrographic and microtextural analyses (Morteani and Grundmann 1977; Grundmann 1983, 1991; Grundmann and Morteani 1982, 1989). All stages depicted pertain to the Alpine metamorphic event

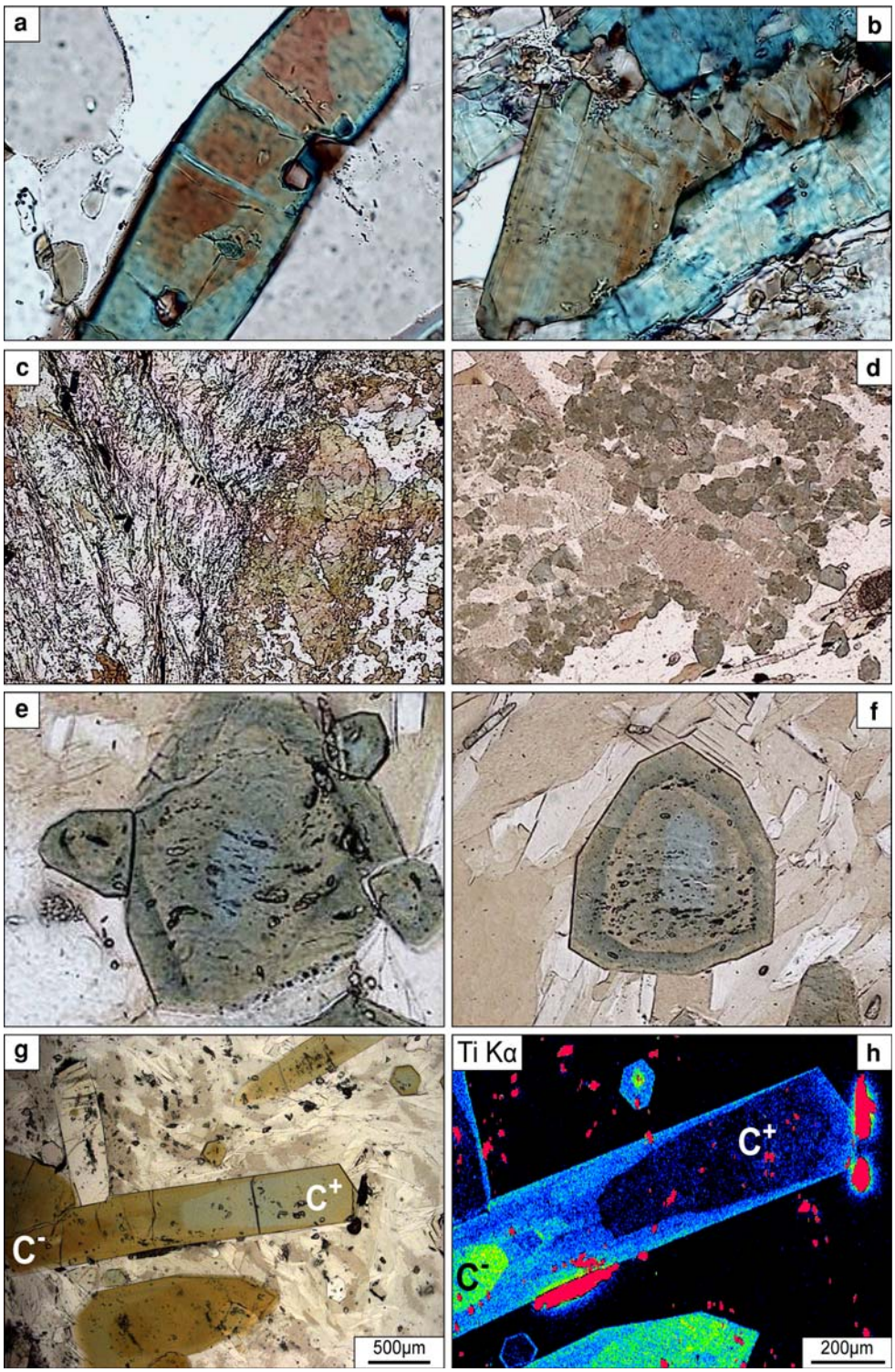

Fig. 4 Representative photomicrographs of tourmaline occurrences in rocks from the Habachtal deposit. **a** Garnet–mica schist (sample 103b) with tourmaline crystals in quartz showing a pre-Alpine broken core (*brown*) which is healed and overgrown by blue Alpine-stage tourmaline, **b** another example of strong brittle deformation in pre-Alpine tourmaline with crack-fillings related to the Alpine event (sample 103b), **c** garnet–mica schist (sample 103b) showing a typical fine grained, polygonal tourmaline aggregate of pre-Alpine age (*brown*), which clearly predates development of the Alpine crenulation cleavage in the rock, **d** tourmaline grain aggregate in biotite–muscovite schist (sample AST-2) showing recrystallization fabrics. Very fine-grained polygonal tourmaline aggregates (*dark brown*) overgrow columnar tourmaline porphyroblasts (*light brown*) indicating strain-induced grain boundary migration and reduction during the Alpine metamorphism, **e** zoned, euhedral tourmaline blast in biotite–chlorite schist from the blackwall zone with sigmoidal inclusion trails indicating tourmaline growth during Alpine deformation, **f** a typical zoned euhedral tourmaline from blackwall biotite–chlorite schist with an inclusion-rich core and inclusion-poor rim, **g** hourglass sector zoning in a tourmaline blast from chlorite schist (sample 103a, grain C–T2). The lighter-colored antigolous pole (C^+) is poor in Ti, Ca and Mg compared with the analogous (C^-) pole, **h** element map of Ti distribution for the sector-zoned crystal shown in **g** acquired by electron microprobe. The warmer colors represent higher Ti concentrations

Boron isotope determination

The boron isotope composition of tourmaline was determined by secondary ion mass spectrometry (SIMS) with the CAMECA ims6f instrument at the GFZ Potsdam. After electron microprobe analysis, the samples were re-polished with alumina and distilled water to remove the carbon coat, then ultrasonically cleaned with high purity ethanol and coated with ~35 nm thick high purity gold coat. The use of a liquid nitrogen cold trap provided a secondary ion source pressure in the lower 10^{-10} Torr range. For the boron isotopic analyses the ims6f was set up in Köhler mode and

employed a nominally 12.5 kV $^{16}O^-$ primary beam which was focused to about 10 μm diameter on the sample surface. Wherever size permitted, both rim and core compositions of individual grains were measured. In two analytical sessions, the beam current was set at 8 or 4 nA, the lower current being required to maintain count rates for ^{11}B below 500 kHz. Prior to each analysis, a 3-min preburn was used in order to remove the gold coat and to establish equilibrium sputtering conditions. The mass spectrometer was operated at mass resolving power $M/\Delta M \approx 1{,}400$, sufficient to separate the isobaric interference of $^{10}B^1H$ on the ^{11}B mass station and the $^9Be^1H$ peak on ^{10}B. A 50 μm diameter contrast aperture, an 1,800 μm field aperture (equivalent to a 150 μm field of view) and 50 V energy window were used without voltage offset. Each analysis consisted of 100 scans of the sequence $^{9.95}$background (0.1 s per cycle), ^{10}B (2 s) and ^{11}B (1 s) resulting in a total analysis time of about 10 min. Instrumental mass fractionation (IMF) and analytical quality were assessed by replicate analyses of tourmaline reference materials dravite (HS #108796), elbaite (HS #98144) and schorl (HS #112566) from the Harvard Mineralogical Museum (Dyar et al. 2001), and tourmaline B4 from Tonarini et al. (2003). During the analytical sessions the 1 SD individual uncertainties were typically ±0.3‰ (Table 1) and the repeatability on reference samples averaged 0.6‰ (1 SD). The variation in observed mass fractionation among the different reference samples was 1.4‰ on average (Table 1), which we believe to be the best estimate for the trueness of the data set. Boron isotope compositions are reported in $\delta^{11}B$ notation ($\delta^{11}B = \{^{11}B/^{10}B_{sample}{}^{corr}/^{11}B/^{10}B_{RM} - 1\} \times 1{,}000$) relative to NBS SRM 951, whose $^{11}B/^{10}B$ ratio is taken as 4.04362 (Catanzaro et al. 1970). The results of the boron isotope and chemical analyses are listed in Table 2 and the full set of microprobe data is available in the electronic repository.

Chemical composition of tourmaline

Given that the Habachtal tourmalines grew in metasomatic zones between serpentinite and pelitic schists, it makes sense to describe their compositional features in terms of the three sample groups: country rock (103b), transitional samples (M-26, AST-2) and blackwall zones (biotite schist 102 and 103c, chlorite schist 103a). All tourmalines classify in the alkali group of Hawthorne and Henry (1999) based on cation proportions in the X-site (Fig. 5a), and they plot on the Mg-rich side of the schorl–dravite join on the Al–Mg–Fe diagram of Henry and Guidotti (1985), within the fields for metapelite–metapsammite rocks (Fig. 5b).

There are significant compositional differences in tourmaline from the three groups of host rocks. The

Table 1 Results of SIMS B-isotope analyses on reference tourmalines

Analysis date	$^{11}B/^{10}B$	1 SD (‰)[a]	IMF[b]	$\delta^{11}B$(‰)[c]
Dravite ($^{11}B/^{10}B = 4.017$ and $\delta^{11}B = -6.6$)				
12/13/2006	3.830	0.35	0.9535	−5.9
12/13/2006	3.828	0.32	0.9530	−6.4
12/13/2006	3.827	0.30	0.9527	−6.7
12/14/2006	3.826	0.30	0.9525	−6.9
12/14/2006	3.825	0.30	0.9522	−7.2
Mean	3.827			−6.6
Repeatability in permil[d]	0.50			
Schorl ($^{11}B/^{10}B = 3.993$ and $\delta^{11}B = -12.5$)				
12/13/2006	3.805	0.31	0.9529	−11.9
12/13/2006	3.803	0.25	0.9524	−12.4
12/14/2006	3.801	0.26	0.9519	−12.9
12/14/2006	3.800	0.29	0.9516	−13.2
Mean	3.802			−12.6
Repeatability in permil[d]	0.58			
Elbaite ($^{11}B/^{10}B = 4.001$ and $\delta^{11}B = -10.4$)				
12/13/2006	3.804	0.36	0.9507	−9.5
12/13/2006	3.805	0.28	0.9509	−9.2
12/13/2006	3.804	0.35	0.9507	−9.5
12/14/2006	3.801	0.34	0.9499	−10.3
12/14/2006	3.796	0.34	0.9487	−11.6
Mean	3.802			−10.0
Repeatability in permil[d]	1.06			
B4 tourmaline ($^{11}B/^{10}B = 4.0078$ and $\delta^{11}B = -8.9$)				
12/13/2006	3.820	0.30	0.9531	−8.4
12/13/2006	3.820	0.29	0.9531	−8.4
12/13/2006	3.818	0.28	0.9526	−9.0
12/14/2006	3.819	0.32	0.9529	−8.7
12/14/2006	3.815	0.31	0.9519	−9.7
Mean	3.818			−8.9
Repeatability in permil[d]	0.57			
Dravite ($^{11}B/^{10}B = 4.017$ and $\delta^{11}B = -6.6$)				
3/26/2007	*3.828*	*0.28*	*0.9530*	*−4.4*
3/26/2007	3.817	0.31	0.9502	−7.3
3/27/2007	3.813	0.37	0.9492	−8.3
3/27/2007	3.818	0.36	0.9505	−7.0
3/27/2007	3.815	0.32	0.9497	−7.8
Mean	3.816			−7.6
Repeatability in permil[d]	0.58			
Schorl ($^{11}B/^{10}B = 3.993$ and $\delta^{11}B = -12.5$)				
3/26/2007	*3.807*	*0.28*	*0.9534*	*−9.9*
3/27/2007	3.793	0.45	0.9499	−13.5
3/27/2007	3.797	0.45	0.9509	−12.5
3/27/2007	3.797	0.45	0.9509	−12.5
Mean	3.796			−12.8
Repeatability in permil[d]	0.61			

Values in italics are outliers and not used in repeatability or IMF calculations

[a] Individual uncertainty for 100 cycles (standard deviation/mean) × 1,000

[b] Instrumental mass fractionation ($^{11}B/^{10}B$ measured/$^{11}B/^{10}B$ RM)

[c] Calculated from ratios corrected with average IMF values of 0.9520 (December 2006) and 0.9506 (March 2007) and $^{11}B/^{10}B = 4.04362$ for NBS SRM 951

[d] Repeatability in permil from multiple analyses of each reference material (standard deviation/mean) × 1,000

Table 2 Chemical analyses and B-isotope ratios of tourmalines from the Habachtal emerald deposit

Sample position	M-26 (phengite schist, transition zone)									AST-2 (biotite–muscovite schist, transition zone)								102 (blackwall bt.–chl. schist)			
	Core	Rim	Rim	Core	Core	Rim	Core	Rim	Core	Rim	Core	Core	Core	Rim	Interior	Interior	Interior	Core	Interior	Rim	Core
SiO_2 (wt.%)	37.6	37.2	37.3	37.3	37.7	37.1	37.8	37.7	37.6	36.9	37.7	37.7	37.6	37.1	37.2	37.6	37.1	36.3	37.1	37.1	36.9
TiO_2	0.17	0.22	0.21	0.22	0.13	0.24	0.26	0.17	0.21	0.50	0.15	0.18	0.21	0.51	0.47	0.09	0.49	0.90	0.22	0.49	0.52
Al_2O_3	31.7	31.7	31.1	31.2	32.0	31.7	31.0	31.4	31.6	30.3	31.7	31.4	30.9	30.8	30.0	31.3	29.8	29.6	31.7	30.0	30.4
MgO	9.82	9.91	9.73	9.88	9.65	9.54	10.24	9.69	9.58	9.13	8.70	9.00	9.22	9.27	9.21	8.89	9.30	8.04	8.67	9.24	7.96
MnO	0.03	0.02	0.02	0.04	0.04	0.03	0.04	0.01	0.04	0.00	0.01	0.02	0.05	0.03	0.00	0.01	0.03	0.00	0.03	0.01	0.02
FeO	3.35	3.25	3.43	3.59	3.09	3.55	3.17	3.52	3.55	5.10	4.37	4.64	5.16	5.05	5.11	4.69	5.47	7.28	4.97	5.18	7.06
Cr_2O_3	0.01	0.00	0.00	0.01	0.01	0.00	0.00	0.00	0.03	0.03	0.01	0.01	0.00	0.00	0.00	0.01	0.01	0.08	0.05	0.09	0.06
CaO	0.71	0.90	0.86	0.95	0.38	0.80	0.62	0.78	0.69	0.99	0.40	0.42	0.28	1.01	1.00	0.34	0.75	0.81	0.37	0.83	0.62
Na_2O	2.44	2.32	2.34	2.36	2.60	2.37	2.53	2.44	2.45	2.35	2.25	2.49	2.74	2.25	2.31	2.51	2.51	2.43	2.43	2.40	2.55
K_2O	0.02	0.01	0.02	0.02	0.01	0.02	0.02	0.02	0.00	0.00	0.01	0.01	0.01	0.01	0.04	0.01	0.01	0.02	0.02	0.02	0.01
F	0.00	0.00	0.00	0.00	0.00	0.00	0.20	0.00	0.00	0.00	0.00	0.00	0.03	0.01	0.00	0.00	0.17	0.37	0.11	0.12	0.20
Cl	0.00	0.00	0.00	0.01	0.00	0.00	0.01	0.00	0.00	0.00	0.02	0.01	0.01	0.00	0.00	0.01	0.00	0.00	0.01	0.01	0.00
Sum	85.8	85.6	85.0	85.6	85.6	85.3	85.9	85.7	85.7	85.3	85.3	85.9	86.2	86.0	85.3	85.5	85.7	85.9	85.6	85.4	86.3
Si (Atoms p.f.u.)	6.087	6.044	6.113	6.086	6.106	6.056	6.132	6.126	6.117	6.093	6.161	6.133	6.114	6.059	6.134	6.151	6.110	6.055	6.059	6.112	6.089
Al (T)	0.000	0.000	0.000	0.000	0.000	0.000	0.000	0.000	0.000	0.000	0.000	0.000	0.000	0.000	0.000	0.000	0.000	0.000	0.000	0.000	0.000
Al (Z)	6.000	6.000	6.000	5.992	6.000	6.000	5.925	6.000	6.000	5.895	6.000	6.000	5.918	5.929	5.838	6.000	5.791	5.819	6.000	5.837	5.907
Al (Y)	0.063	0.083	0.010	0.000	0.122	0.106	0.000	0.025	0.047	0.000	0.104	0.028	0.000	0.000	0.000	0.030	0.000	0.000	0.114	0.000	0.000
Ti	0.021	0.027	0.026	0.027	0.016	0.029	0.032	0.020	0.026	0.062	0.019	0.022	0.026	0.063	0.059	0.011	0.060	0.113	0.027	0.060	0.064
Mg	2.372	2.401	2.378	2.401	2.330	2.321	2.476	2.348	2.321	2.244	2.117	2.183	2.234	2.256	2.264	2.165	2.281	1.995	2.113	2.270	1.958
Mn	0.003	0.003	0.003	0.005	0.006	0.004	0.005	0.002	0.005	0.000	0.001	0.002	0.006	0.004	0.000	0.002	0.004	0.000	0.004	0.001	0.003
Fe	0.454	0.442	0.470	0.489	0.419	0.485	0.430	0.479	0.483	0.704	0.597	0.631	0.702	0.690	0.705	0.642	0.753	1.014	0.680	0.715	0.975
Cr	0.001	0.000	0.000	0.001	0.001	0.000	0.000	0.000	0.002	0.002	0.001	0.001	0.000	0.000	0.000	0.001	0.001	0.005	0.003	0.006	0.004
Ca	0.123	0.156	0.152	0.166	0.066	0.139	0.108	0.135	0.120	0.174	0.070	0.074	0.049	0.177	0.176	0.060	0.131	0.145	0.064	0.146	0.109
Na	0.767	0.730	0.743	0.746	0.817	0.750	0.796	0.770	0.773	0.751	0.711	0.787	0.865	0.712	0.740	0.796	0.800	0.785	0.771	0.769	0.816
K	0.004	0.002	0.004	0.004	0.002	0.004	0.003	0.005	0.000	0.000	0.002	0.002	0.003	0.001	0.008	0.001	0.003	0.005	0.004	0.005	0.002
Vacancies	0.105	0.112	0.101	0.085	0.115	0.106	0.092	0.090	0.107	0.075	0.218	0.138	0.084	0.109	0.076	0.143	0.066	0.065	0.161	0.081	0.073
$^{11}B/^{10}B$	4.013	4.003	3.991	3.994	4.001	4.000	4.000	3.994	3.995	3.995	4.002	4.006	4.019	3.992	4.013	4.004	4.016	4.022	4.011	4.018	4.022
1σ Uncertainty (‰)	0.36	0.36	0.35	0.31	0.36	0.32	0.38	0.33	0.35	0.33	0.31	0.34	0.32	0.35	0.34	0.32	0.35	0.33	0.34	0.29	0.35
$\delta^{11}B$ (‰)	−7.7	−10.0	−13.1	−12.3	−10.5	−10.8	−10.8	−12.3	−12.1	−12.1	−10.3	−9.2	−6.1	−12.9	−7.7	−9.7	−6.9	−5.3	−8.2	−6.4	−5.3

Table 2 continued

Sample position	103c (Blackwall bt. schist)				103a (Blackwall chlorite schist)										103b (Country rock ga.–mu. schist)			
	Rim	Interior	Rim	Core	Rim	Core	Rim	Core	Rim	Core	Rim	Rim	Rim	Core	Interior	Interior	Core	core
SiO_2 (wt.%)	37.0	37.0	37.3	37.2	37.3	37.3	37.4	37.3	37.5	37.7	37.4	37.1	37.4	37.3	37.0	36.7	37.1	37.2
TiO_2	0.50	0.60	0.50	0.35	0.43	0.32	0.52	0.13	0.47	0.20	0.22	0.60	0.35	0.10	1.07	0.90	0.71	0.66
Al_2O_3	30.1	30.5	30.8	30.5	30.2	30.2	30.8	31.5	30.7	31.4	31.7	30.5	30.6	31.3	31.8	32.3	33.2	32.7
MgO	9.42	9.37	9.71	9.17	9.59	9.35	9.67	8.68	9.88	8.97	8.91	9.58	9.60	8.54	6.31	6.44	6.18	5.60
MnO	0.00	0.02	0.02	0.06	0.00	0.01	0.00	0.01	0.00	0.00	0.03	0.01	0.01	0.00	0.04	0.06	0.06	0.09
FeO	4.97	4.71	3.97	5.55	3.91	4.05	3.85	4.34	3.86	4.22	4.33	3.95	3.91	5.36	8.33	7.94	7.54	8.11
Cr_2O_3	0.06	0.04	0.03	0.04	0.06	0.03	0.03	0.01	0.07	0.02	0.05	0.08	0.06	0.03	0.10	0.00	0.03	0.01
CaO	0.87	0.66	0.98	0.54	0.90	0.75	1.09	0.26	0.94	0.35	0.28	1.03	0.78	0.12	0.79	1.06	0.99	0.77
Na_2O	2.45	2.53	2.30	2.55	2.51	2.58	2.24	2.48	2.41	2.45	2.49	2.30	2.58	2.71	2.11	1.99	1.87	1.86
K_2O	0.02	0.02	0.03	0.03	0.02	0.00	0.02	0.03	0.02	0.00	0.01	0.02	0.02	0.02	0.02	0.03	0.02	0.02
F	0.03	0.25	0.21	0.04	0.32	0.21	0.31	0.00	0.41	0.09	0.14	0.27	0.25	0.00	0.00	0.00	0.00	0.00
Cl	0.00	0.01	0.00	0.01	0.01	0.00	0.01	0.00	0.00	0.00	0.01	0.01	0.01	0.00	0.01	0.00	0.01	0.01
Sum	85.4	85.7	85.9	86.1	85.3	84.7	85.9	84.8	86.2	85.3	85.5	85.4	85.6	85.5	87.6	87.5	87.7	87.0
Si (Atoms p.f.u.)	6.094	6.080	6.088	6.074	6.165	6.186	6.121	6.143	6.107	6.162	6.111	6.104	6.136	6.114	6.052	5.999	6.032	6.105
Al (T)	0.000	0.000	0.000	0.000	0.000	0.000	0.000	0.000	0.000	0.000	0.000	0.000	0.000	0.000	0.000	0.001	0.000	0.000
Al (Z)	5.844	5.899	5.939	5.881	5.877	5.898	5.930	6.000	5.903	6.000	6.000	5.921	5.928	6.000	6.000	6.000	6.000	6.000
Al (Y)	0.000	0.000	0.000	0.000	0.000	0.000	0.000	0.113	0.000	0.049	0.096	0.000	0.000	0.053	0.130	0.228	0.352	0.323
Ti	0.062	0.075	0.061	0.043	0.054	0.040	0.064	0.016	0.057	0.024	0.027	0.074	0.044	0.013	0.131	0.111	0.086	0.081
Mg	2.312	2.293	2.365	2.232	2.360	2.312	2.356	2.129	2.401	2.187	2.168	2.352	2.349	2.085	1.537	1.568	1.496	1.367
Mn	0.000	0.003	0.003	0.009	0.000	0.001	0.000	0.001	0.000	0.000	0.004	0.001	0.002	0.000	0.005	0.008	0.008	0.012
Fe	0.684	0.647	0.542	0.758	0.541	0.562	0.526	0.598	0.527	0.577	0.591	0.545	0.537	0.734	1.139	1.084	1.024	1.112
Cr	0.004	0.002	0.002	0.003	0.004	0.002	0.002	0.001	0.004	0.001	0.003	0.005	0.004	0.002	0.006	0.000	0.002	0.001
Ca	0.153	0.116	0.172	0.094	0.159	0.133	0.190	0.046	0.164	0.062	0.050	0.182	0.138	0.020	0.139	0.186	0.172	0.135
Na	0.781	0.805	0.729	0.807	0.803	0.829	0.710	0.790	0.762	0.778	0.788	0.735	0.822	0.862	0.667	0.630	0.589	0.590
K	0.004	0.004	0.005	0.007	0.004	0.001	0.003	0.006	0.004	0.001	0.002	0.003	0.005	0.003	0.003	0.007	0.005	0.004
vacancies	0.062	0.075	0.093	0.092	0.034	0.037	0.097	0.158	0.070	0.159	0.161	0.079	0.036	0.115	0.191	0.177	0.235	0.271
$^{11}B/^{10}B$	4.016	4.018	4.005	4.015	4.008	4.020	4.007	4.011	4.007	4.022	4.020	4.002	4.005	4.023	4.004	3.989	3.996	3.996
1σ Uncertainty (‰)	0.30	0.32	0.33	0.33	0.32	0.33	0.32	0.32	0.30	0.32	0.29	0.34	0.31	0.32	0.38	0.28	0.35	0.35
$\delta^{11}B$ (‰)	−6.9	−6.4	−9.5	−7.1	−8.7	−5.8	−9.0	−8.2	−9.0	−5.3	−5.8	−10.3	−9.5	−5.1	−9.8	−13.5	−11.7	−11.7

Chemical analyses by electron microprobe, total Fe reported as FeO, structural formula based on 15 cations in T, Z and Y sites (Henry and Dutrow 1996)

B-isotope ratios by SIMS on points adjacent to microprobe sites, corrected for instrumental mass fractionation (Table 1) and with 1 σ individual uncertainty given in permil

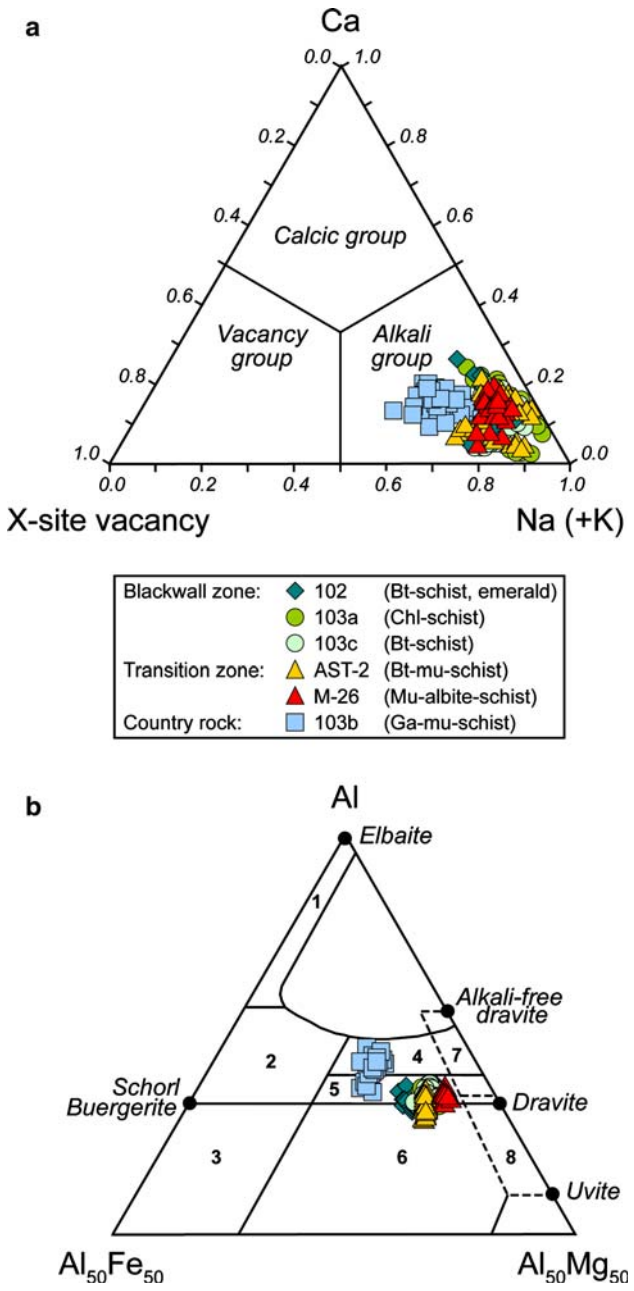

Fig. 5 Classification diagrams for the tourmalines from the Habachtal deposit, based on the principal constituent at the X-site (Hawthorne and Henry 1999) in (**a**) and on the Al–Fe–Mg ternary diagram from Henry and Guidotti (1985) in (**b**). The labeled fields in plot **b** are: (1) Li-rich granitoid pegmatites and aplites, (2) Li-poor granitoids, pegmatites and aplites, (3) Fe^{3+}-rich quartz–tourmaline rocks (altered granitoids), (4) metapelites and metapsammites with Al-saturating phase, (5) metapelites and metapsammites lacking Al-saturating phase, (6) Fe^{3+}-rich quartz–tourmaline rocks, calc-silicate rocks and metapelites, (7) low-Ca metaultramafic rocks and Cr–V-rich metasediments, (8) metacarbonates and metapyroxenites

Fe/(Fe + Mg) ratio is among the most distinct of these (Fig. 6a), with values declining from the country rocks to the blackwall biotite and chlorite schist, in good agreement with the whole-rock ranges shown on the diagram (data from Grundmann 1983). One of the two transitional zone samples (biotite–muscovite schist AST-2) has Fe/(Fe + Mg) ratios intermediate between those in the country rock and blackwall tourmalines as expected for its position in the sequence. However, the other one (albite-muscovite schist M-26) has the lowest ratios of all samples. This is thought to reflect the protolith composition and not the effect of blackwall alteration since the rock represents a fragment of pre-Alpine whiteschist (G. Morteani personal communication) which is rich in magnesian phengite. Also distinctive of tourmalines from the blackwall zones are their moderate to high fluorine contents, which contrast with the low or negligible F in tourmalines from the country rock and transitional samples (Fig. 6b). Further, the blackwall tourmalines show a wide range of Ca and Ti concentrations (0.2–1.4 wt.% CaO and 0.1–0.8 wt.% TiO_2) with a strong positive correlation between the two (Fig. 6c). The country rock tourmalines have a greater scatter of TiO_2 and CaO values (Fig. 6c). Note that the whiteschist tourmalines (M-26) form a separate cluster at low TiO_2 on this diagram. Finally, Al concentrations are higher in tourmalines from the metapelite country rock than in the blackwall zones (Fig. 7a), and these Al-rich tourmalines also have relatively high values for the X-site vacancy, up to 30% (Figs. 5a, 7b). The good correlations of Fe versus total Al and Fe versus X-site vacancy in these tourmalines, and the slope of data trends compared with the exchange vectors shown on Fig. 7, illustrate the importance of the "alkali-deficient" exchange component $\{(Na,Fe)(\square,Al_{-1})\}$ for charge-balancing the excess aluminum.

One might expect high Cr contents in tourmalines from emerald-bearing blackwall rocks compared to those in the country rocks and the average values of both groups of samples bear this out (0.05 wt.% Cr_2O_3 for blackwall samples, 0.02 wt.% for garnet–mica schist). However, the scatter is large in the both groups and the maximum Cr_2O_3 content of blackwall tourmalines is only a moderate 0.14 wt.% (Appendix A of ESM). These values are similar to those of blackwall-hosted tourmalines studied by Altherr et al. (2004) and Marschall et al. (2006) but they are quite low compared with tourmalines from other emerald-bearing rocks in the literature. Seifert et al. (2004) reported maxima of 1–2.7 wt.% Cr_2O_3 from tourmaline coexisting with emerald in blackwall metasomatic rocks (phlogopite–talc–actinolite) from Zambia, and tourmalines from the Tsa da Glisza (Regal Ridge) emerald prospects in Yukon Territory reach similarly high Cr_2O_3 concentrations, with a maximum of 3.3 wt.% (Groat et al. 2002; C.G. Galbraith personal communication).

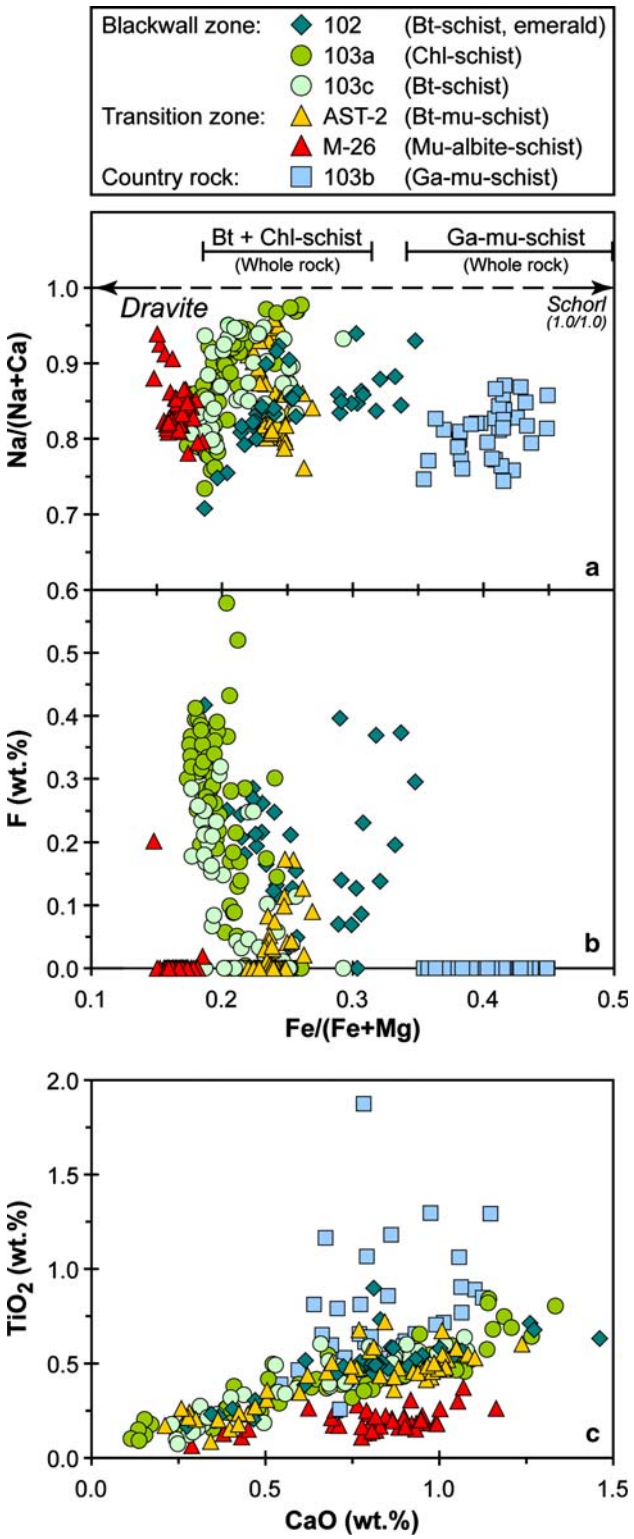

Fig. 6 Chemical compositions of tourmalines from the Habachtal deposit expressed in terms of the atomic ratios Fe/(Fe + Mg) versus **a** Na/(Na + Ca) and **b** F (wt.%); and in **c** contents of CaO (wt.%) versus TiO_2 (wt.%). Whole-rock ranges shown in **a** are from data in Grundmann (1983)

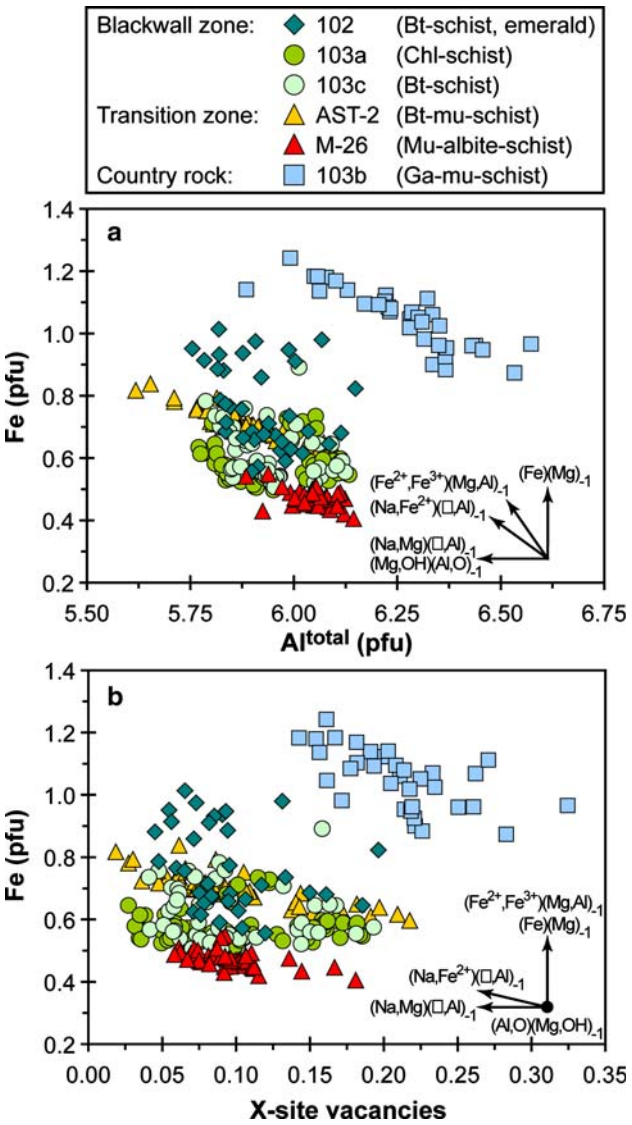

Fig. 7 Compositional variation diagrams of **a** total Al (atoms per formula unit) and **b** X-site vacancies versus Fe (atoms p.f.u.); exchange vectors are indicated by arrows (*open square*—vacancy)

Compositional zoning as a monitor of blackwall alteration

As described above, the pre-Alpine fine-grained grains and grain aggregates from the country rocks and transition zone samples have weak and simple optical zoning (Fig. 4d), and microprobe analyses from this type of tourmaline show little or no consistent variations in core versus rim compositions (Table 2, Appendix A of ESM). On the other hand, most tourmaline grains from the blackwall schists display distinct optical zoning (Fig. 4e, f) and have systematic compositional zoning as well. Typically, the rims of zoned grains are enriched in Mg, Ti, Ca and F relative to

the cores (Fig. 8). Rims may show relative depletion in Na, Fe and Al, but the trends for these elements are less regular. Zoned emeralds in these rocks also display consistent trends of higher Mg/(Mg + Fe) ratios and lower Al contents from core-to-rim (Grundmann 1983).

It is significant that the core-to-rim compositional variations in the blackwall tourmalines mirror the overall changes in tourmaline composition from the country rocks into the blackwall alteration zones, implying that the compositional changes in zoned grains record the changing fluid composition as blackwall alteration progresses. The lithologic and petrographic characteristics of the blackwall sequence support this interpretation. First, microtextures and inclusion fabric of emerald and tourmaline porphyroblasts indicate that the main period of growth for both phases was syn-deformational and followed by static growth of the relatively narrow rims (Fig. 3). This growth is prograde, as indicated by fluid inclusion microthermometry from zoned emeralds by Nwe and Grundmann (1990), with peak metamorphic temperatures of 500–550°C. Second, whole-rock geochemistry (Grundmann and Morteani 1989) established that the original contact between serpentinite and the country rocks was at the present boundary between chlorite schist and actinolite–talc schists (Fig. 2). This means that the chlorite and biotite blackwall schists were once metapelites and that their core-to-rim chemical zonation is equivalent to a time sequence of advancing metasomatism.

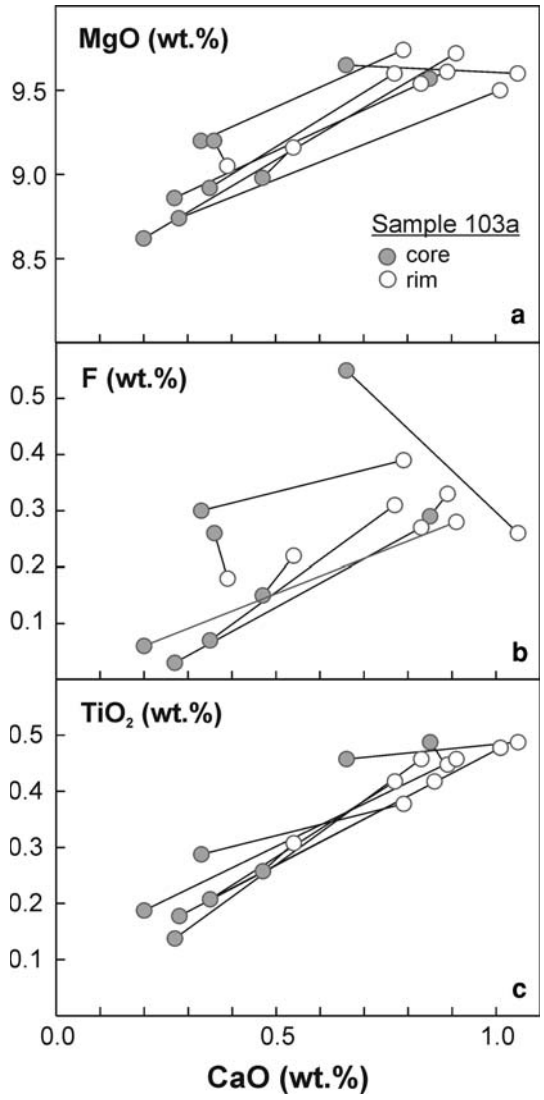

Fig. 8 An example of tourmaline compositional zoning from blackwall-zone samples. The tielines connect core and rim compositions of individual tourmaline grains analyzed in sample 103a (chlorite schist)

A special feature of tourmalines from the chlorite–biotite schist (sample 103a) is hourglass sector zoning (Fig. 4g,h), which is unusual for tourmaline and was described in detail by van Hinsberg et al. (2006). Although common in tourmalines from sample 103a, hourglass zonation is not developed in any of the other samples examined in this study. Why this is so is not known. The sector zoning in tourmaline is interesting because the mineral's polar properties cause a compositional and color contrast between the C^- (analogous) and C^+ (antilogous) poles (Fig. 4g). The sector-zoned tourmalines from sample 103a show the typical variations in Ti and Ca on opposite ends of the *C*-axis, leading to a clear color contrast like those from other localities described by van Hinsberg et al. (2006). We did not perform detailed microprobe traverses across these crystals but instead illustrate their compositional variations with a Ti distribution map from a large and well-developed example in Fig. 4h. Spot analyses on this and other zoned grains in the sample demonstrate a contrast in CaO and TiO_2 concentrations at the C^+ versus C^- sectors of about 0.5 wt.%. Henry and Dutrow (1996) suggested that the bipolar effect is significant only in tourmalines from low-temperature conditions but the work of van Hinsberg et al. (2006, 2007) shows that zoning can persist to the amphibolite grade and this is confirmed by the Habachtal tourmalines, which formed at temperatures of at least 500°C (Nwe and Grundmann 1990). Van Hinsberg and Marschall (2007) found that sector-zoned tourmaline crystals can show a slight but significant variation in B-isotope composition between the C^+ and C^- sectors. Our SIMS analyses on the sector-zoned Habachtal crystals confirm a weak isotopic effect as described below.

Boron isotope results

The total range in boron isotope compositions for tourmalines from the country rock schist to the metasomatic rocks of the blackwall zones is from −13.8 to −5.1‰ in the $\delta^{11}B$ notation (Fig. 9; Table 2). These isotopically

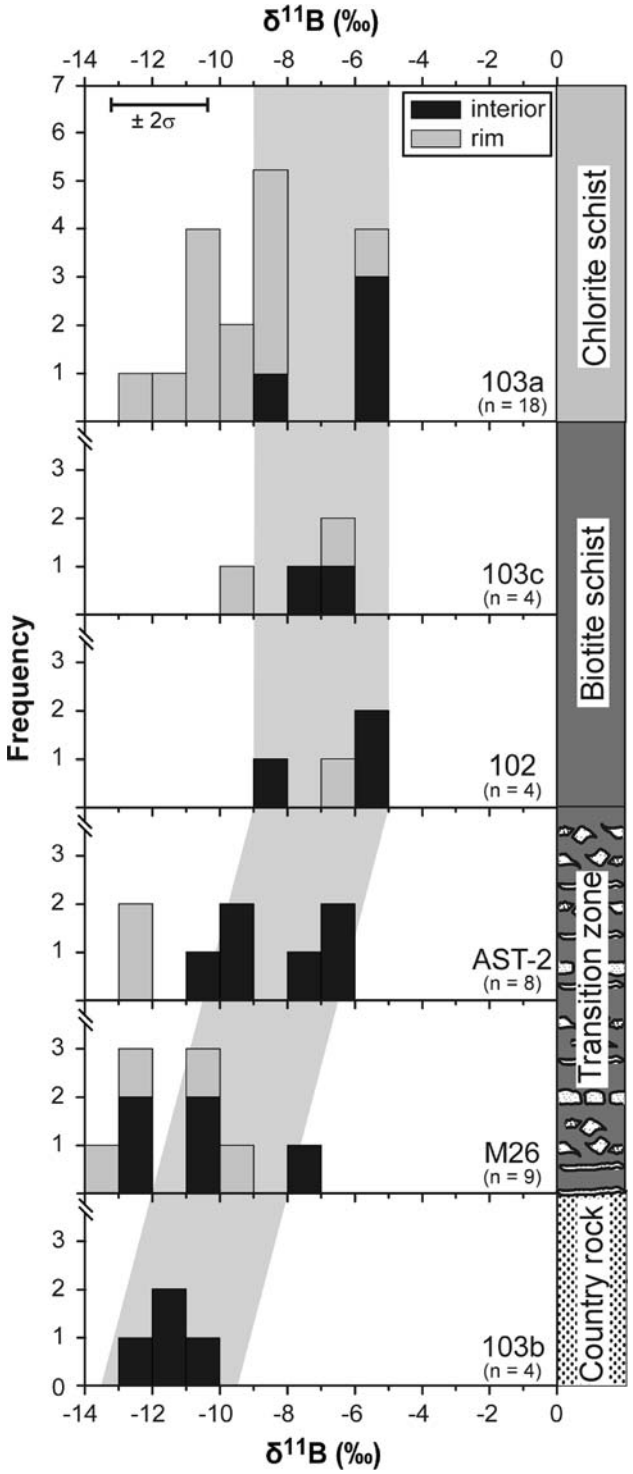

Fig. 9 Frequency histograms of boron isotope compositions of Habachtal tourmalines from the country rock, transition zone and blackwall-zone samples. The core and rim compositions of zoned grains are shown separately. The error bar in the upper panel illustrates the analytical repeatability of SIMS analyses at the 2σ level. The shaded zone emphasizes the observed trend to higher $\delta^{11}B$ values with increasing intensity of blackwall alteration. This trend is found only in tourmaline cores, meaning a shift in fluid composition during tourmaline growth

light values are well within the range of tourmalines from metasedimentary rocks reported from other studies (Palmer and Swihart 1996; Kasemann et al. 2000; Bebout and Nakamura 2003; Trumbull et al. 2008), and they contrast with the heavy B-isotope values of tourmaline from eclogite–serpentinite mélange rocks in Turkey (−2.2 to +1.7‰) reported by Altherr et al. (2004), and in Syros (+18 to +28‰) found by Marschall et al. (2006). Both of those studies attributed the isotopically heavy boron to a fluid source in the subducted oceanic slab, which in the case of Syros was further modified during fluid migration through and interaction with serpentinites above the slab.

The most significant features of the Habachtal isotope data are summarized here and their possible implications for the fluid source and mineralization process are discussed in the following section.

1. There is an overall shift in the B-isotope compositions of tourmaline from more negative $\delta^{11}B$ values in the country rock samples to less negative values in the blackwall zones (Fig. 9). The differences in composition between country rock and blackwall zones are largest and most consistent with respect to the core compostions.
2. The variations in $\delta^{11}B$ within individual samples is typically 3–5‰, which is considerably greater than the analytical uncertainty and therefore an indication for a heterogeneous boron source and/or processes of isotopic fraction connected with tourmaline growth in these rocks.
3. Isotopic variations from core-to-rim of zoned tourmaline grains were not found in the country-rock tourmalines, but there are examples of significant isotopic zoning in some of the transitional zone and blackwall samples (Table 2). The core-rim isotopic contrast rarely exceeds 2‰; however, the trends of isotope zoning are mostly the same, with tourmaline rims being isotopically lighter than the cores (Fig. 9). Tourmaline in sample 103a (chlorite schist), which shows the strongest optical and chemical zonation (Fig. 8), also has the strongest isotopic zonation of all samples, at 4‰.
4. Tourmaline grains with well-developed hourglass sector zoning in sample 103a were checked for B-isotope variations by analyzing two points on each of the C^+ and C^- sectors in two separate grains (Appendix B of ESM). The results showed minor but significant isotopic differences. Specifically, grain "C–T2" (Fig. 4g, h) yielded two identical values for the C^+ zone (−10.9‰) whereas the C^- values were −12.0 and −12.5‰, giving an average contrast of 1.3‰. For grain "D–T1", the C^+ sector yielded −8.0 and −8.3‰ and the C^- values were

−9.3 and −10.1‰, for an average contrast of 1.5‰. These differences exceed both the SIMS repeatability error of about 0.6‰ (Table 1) and the individual uncertainties calculated by error propagation [$\sigma_{a+b} = (\sigma a^2 + \sigma b^2)^{1/2}$]. Furthermore, the sense of variation is the same in both grains, with isotopically lighter boron at the C^- sector, in agreement with the findings of van Hinsberg and Marschall (2007). The reason for an isotopic contrast between the two sectors is presently not understood and it deserves further study. However, the effect is too weak to complicate the overall interpretation of this study and sector zoning affects only one sample.

Discussion: B-isotope variations and implications for the fluid source

Two features of the tourmaline $\delta^{11}B$ results stand out as most significant in their implications for fluid-rock interaction in the Habachtal deposit. The first is the observed variation by up to 6‰ in the isotope composition within individual samples. In many cases this internal variation is partly due to isotopic zoning, which is typically on the order of 2‰ and involves lower $\delta^{11}B$ values in rims relative to cores. The strongest isotopic zoning of about 4‰ was found in tourmalines from the inner blackwall zone (chlorite schist 103a), which is the sample representing the most advanced metasomatism. The second important feature is a systematic difference in the B-isotope composition depending on location of the samples in the shear zone/alteration sequence. Tourmaline from the country rock metapelite has low $\delta^{11}B$ values (−13 to −10‰), typical for continental crust whereas the blackwall-zone tourmalines are isotopically heavier, reaching −5‰ in $\delta^{11}B$ (Fig. 9). Furthermore, these spatial differences among the samples are best developed in the tourmaline core compositions, as emphasized by the shaded band on Fig. 9, meaning that they relate to the fluid–rock system during the main stage of tourmaline growth in the shear zone.

In principle, the observed B-isotope variations in Habachtal tourmalines can relate to one or both of two factors: local conditions that cause isotopic fractionation between fluid and growing crystals (closed-system, single initial fluid composition); or an open-system behavior with more than one fluid composition controlling the B-isotopes. Obviously, some open-system behavior is expected for a ductile shear zone with strong metasomatic alteration and meter-thick quartz veins, but we will first consider what range of B-isotopic variations can be expected from fluid–mineral fractionation processes and temperature gradients acting on an initially constant fluid composition. For the Habachtal rocks, the important minerals to consider are not only tourmaline but potentially also biotite and chlorite, since the blackwall biotite and chlorite schists consist of more than 90 vol.% of these minerals. The condition for partitioning of B-isotopes between phases is a change in the coordination environment of boron, with ^{10}B being enriched in tetrahedral sites and ^{11}B in trigonal coordination. In addition, the fractionation effect is inversely dependent on temperature. Boron in hydrothermal fluids occurs in trigonal $B(OH)_3$ complexes at the low pH conditions suitable for tourmaline stability (Palmer and Swihart 1996; Schmidt et al. 2005). Boron in tourmaline forms trigonal BO_3 groups whereas it replaces Al in tetrahedral sites in the sheet silicates. Experimental studies are available for B-isotope fractionation between fluid–tourmaline (Palmer et al. 1992; Meyer et al. 2008), fluid–clay (Williams et al. 2001) and fluid–muscovite (Wunder et al. 2005).

Application of the isotope partitioning studies to the Habachtal tourmalines requires temperature information. The Variscan regional metamorphism in the Tauern Window reached peak temperatures estimated at 450°C (Grundmann 1989). These conditions are thought to be relevant for tourmalines in the country rock metapelites, whereas the main stage of tourmaline and emerald growth, along with blackwall alteration and quartz veining in the Habachtal deposit, took place during Alpine metamorphism, with peak temperatures of about 550°C (Grundmann 1989 and references therein). At a temperature of 550°C, the B-isotope fractionation between hydrothermal fluid and tourmaline would be about −4‰ according to Palmer et al. (1992) or about −2‰ using the results of Meyer et al. (2008). For comparison, the fluid–mica fractionation at the same temperature would be about −10‰ (Wunder et al. 2005). If we assume for discussion that the 100°C difference between the Variscan and Alpine peak conditions is the maximum temperature range to be expected for tourmaline growth in Habachtal, the corresponding shift in $\delta^{11}B$ would be about 2 or 1‰ depending on which experimental results are used. In any case, the expected temperature effect is less than the within-sample range of 3–6‰ and much less that the variation of 8‰ between the country rock and the inner blackwall zone. Also, temperature variations during tourmaline growth can be ruled out as the cause of isotopic zoning since crystal growth is prograde so the predicted temperature effect would cause higher $\delta^{11}B$ values from core-to-rim, which is contrary to observation. We conclude that temperature cannot be a controlling factor in the isotopic variations observed although it may contribute to the scatter of values within samples.

Another commonly cited mechanism for changing the isotopic composition of tourmaline is a Rayleigh-type fractionation, whereby mineral growth depletes the fluid

reservoir in boron and preferentially in ^{10}B, causing progressively heavier B-isotopic compositions in the remaining fluid and late-stage tourmalines. Rayleigh fractionation was invoked to explain isotopic zoning in tourmalines by Trumbull et al. (2008) but it is not likely to be significant for the Habachtal example because of the high fluid/rock ratios evidenced by monomineralic chlorite and biotite schist zones and meter-wide quartz veins. Moreover, the observed isotopic variation in zoned tourmalines argues against Rayleigh fractionation because that process should cause isotopically heavier tourmaline rims, whereas zoned grains show the opposite trends.

We have shown that the observed shifts in B-isotopic composition among the Habachtal samples and within zoned grains cannot be explained by fractionation processes or temperature gradients alone and so there must be significant time–space variations in the fluids of contrasting B-isotope composition. There is independent evidence for changing fluid compositions at Habachtal from a study of fluid inclusions in zoned emerald crystals by Nwe and Grundmann (1990). These authors distinguished an early and late generation of primary inclusions which differ primarily in terms of fluid density and the proportion of CO_2 ($X_{CO_2} < 4$ vol.% in the early generation and up to 11 vol.% in later fluids). The important conclusions from that study are that the aqueous and carbonic fluids represent simultaneous trapping of heterogeneous fluids, and that variations in fluid density reflect changing conditions of hydrostatic versus lithostatic pressure in the ductile shear zone. Nwe and Grundmann (1990) attributed the higher CO_2 contents in the later fluid inclusions to consumption of H_2O by hydration reactions during advancement of the metasomatic front. Given the close association of emerald and tourmaline porphyroblasts in the blackwall zones and the similarity of their inclusion assemblages and zoning patterns, we can assume that the tourmalines studied here experienced the same fluctuations in fluid pressure and composition during growth.

There must be at least two isotopically distinct sources of boron to explain the variations in tourmaline isotope composition across the blackwall zones and within the growing crystals. The B-isotope composition of garnet-mica schist-hosted tourmaline in the country rocks (−13 to −10‰) is a typical value for continental metasediments (Palmer and Swihart 1996; Kasemann et al. 2000) and one component in the Habachtal fluid–rock system is suggested to be crustal metamorphic fluid with this range of composition. The other boron source needed to explain the tourmaline data must be isotopically heavy, and a conservative estimate for this component is −3‰ based on the highest observed $\delta^{11}B$ values of −5‰ and using fluid–tourmaline fractionation factors for 500°C. This composition is in the range for MORB and altered oceanic crust (Palmer and Swihart 1996) and given the geologic setting, the likely source of isotopically heavy boron is the serpentinite and metabasic rocks in the Habach Group (compare Altherr et al. 2004; Marschall et al. 2006). In support of this suggestion is the regional association of blackwall alteration and serpentinite bodies in the Tauern Window distributed along the Greiner shear zone (Fig. 1a), which are interpreted as remnants of oceanic lithosphere caught up during the Alpine orogeny (Melcher et al. 2002). Barnes et al. (2004) argued from H and O isotope evidence that dehydration of serpentinites was an important source of fluids for blackwall-type metasomatism in the western Greiner shear zone, and this is consistent with our B-isotope results from the Habachtal.

We therefore propose that the main control on B-isotope variations in the Habachtal tourmalines is related to changing proportions of fluids from these two contrasting sources. The progressive shift toward heavier $\delta^{11}B$ values from the country rock through transitional samples and into the blackwall alteration zones (Fig. 9) reflects the increasing fluid/rock ratios and greater dominance of heavy boron from the serpentinite/metabasite component. The isotopic scatter within individual samples can be explained by changing proportions of the component fluids in the shear zone with additional variations resulting from fractionation effects related to mineralization (of biotite, particularly) and increasing temperature. The trend toward isotopically lighter B in the rims of zoned tourmalines, which is observed in the blackwall and in the transitional samples, suggests a greater role of the regional metamorphic fluid at peak conditions.

Conclusions

The Habachtal emerald deposit is the type example of schist-hosted emerald deposits related to regional metamorphism. Deformation-enhanced metasomatic reactions between serpentinite and metapelitic country rocks in a ductile shear zone produced meter-thick “blackwall” alteration zones of biotite and chlorite schists which host the emerald mineralization. Tourmaline occurs in association with emerald in the blackwall zones and it is also a common accessory mineral in the country rock garnet–mica schists. Electron microprobe and SIMS analyses of tourmalines from an idealized profile across the blackwall sequence reveals systematic chemical and B-isotopic variations. Systematic chemical variations in tourmaline from unaltered country rock through transitional samples and into the nearly monomineralic biotite and chlorite schists from the blackwall zones (decreasing Al and Fe/(Mg + Fe) ratio, increasing F and Cr) parallel changes in bulk composition of the rocks. Optical zoning is well

developed in the blackwall tourmalines, and many grains also show strong compositional zoning, with increasing Mg, Ti, Ca and F concentration and decreasing Na and Al from core-to-rim, which mimics the differences found in the spatial sequence of blackwall zones. A special feature of some metasomatic tourmalines in the chlorite schist zone is development of hourglass sector zoning, with enrichments of Ti and Ca on oppposite ends of the *C*-axis. B-isotopic variations between the C^+ and C^- sectors of these tourmalines are weak but significant, with a contrast on the order of 1.5‰.

The total range in B-isotope composition of Habachtal tourmalines is from −13.8 to −5.1‰ in the $\delta^{11}B$ notation. Many of the optically and chemically zoned tourmalines from the blackwall and transitional zones also show a consistent trend of isotopic zoning, with the rims being isotopically lighter than the cores. The largest within-grain variation found was 4‰ but typically, the core-rim differences are about 1.5–2‰. Isotopic zoning is important, because when the core compositions are compared we find a systematic shift in $\delta^{11}B$ values of tourmalines from the country rock (−14 to −10‰) to the inner blackwall zones (−9 to −5‰). This difference cannot be explained by Rayleigh fractionation or temperature variations, and we conclude there must be at least two contrasting boron sources. The simplest model that fits observed tourmaline compositions and is consistent with the geologic setting invokes two separate fluids that were channeled and partially mixed in the shear zone which hosts the Habachtal deposit. One is a regional metamorphic fluid with isotopically light boron as in the metapelite country rocks, and the other fluid is derived from the serpentinite association, which has isotopically heavy boron as in MORB or altered oceanic crust.

Acknowledgments Several colleagues at the GFZ Potsdam contributed their technical expertise to this project. Gerhard Berger prepared the excellent polished thin sections, Oona Appelt set up and helped run the electron microprobe analyses and Ilona Schäpan assisted in the SIMS laboratory. Our special thanks go to Dieter Rhede for performing the high-resolution element mapping with the JEOL Hyperprobe. We are grateful for helpful reviews by Horst Marschall and Bill Leeman, which led to significant improvements in the paper.

References

Altherr R, Topuz G, Marschall H, Zack T, Ludwig T (2004) Evolution of a tourmaline-bearing lawsonite eclogite from the Elekdag area (Central Pontides, N Turkey): evidence for infiltration of slab-derived B-rich fluids during exhumation. Contrib Mineral Petrol 148:409–425

Barnes JD, Selverstone J, Sharp Z (2004) Interactions between serpentinite devolatilization, metasomatism and strike-slip strain localization during deep-crustal shearing in the Eastern Alps. J Metab Geol 22:283–300. doi:10.1111/j.1525-1314.2004.00514.x

Bebout GE, Barton MD (2002) Tectonic and metasomatic mixing in a highT subduction-zone mélangeinsights into the geochemical evolution of the slab-mantle interface. Chem Geol 187:79–106. doi:10.1016/S0009-2541(02)00019-0

Bebout G, Nakamura E (2003) Record in metamorphic tourmalines of subduction-zone devolatilization and boron cycling. Geology 31:407–410. doi :10.1130/0091-7613(2003)031<0407:RIMTOS>2.0.CO;2

Bucher K, de Capitani C, Grapes R (2005) The development of a margarite-corundum blackwall by metasomatic alteration of a slice of mica schist in ultramafic rocks, Kvesjoen, Norwegian Caledonides. Can Mineral 43:129–156. doi:10.2113/gscanmin.43.1.129

Catanzaro EJ, Champion CE, Garner EL, Maienko G, Sappenfield KM, Shields WR (1970) Boric acid: isotopic and assay standard reference materials. National Bureau Standards (US). Spec Publ 260–17:70 p

Christensen JN, Selverstone J, Rosenfeld J, dePaolo DJ (1994) Correlation by Rb-Sr geochronology of garnet growth histories from different structural levels within the Tauern Window, Eastern Alps. Contrib Mineral Petrol 118:1–12. doi:10.1007/BF00310607

Cliff RA (1981) Pre-Alpine history of the Pennine zone in the Tauern Window, Austria: U-Pb and Rb-Sr geochronology. Contrib Mineral Petrol 77:262–266. doi:10.1007/BF00373541

Curtis CD, Brown PE (1969) The metasomatic development of zoned ultrabasic bodies in Unst, Shetland. Contrib Mineral Petrol 24:275–292. doi:10.1007/BF00371271

Dyar MD, Wiedenbeck M, Robertson D, Cross LR, Delaney JS, Ferguson K et al (2001) Reference minerals for microanalysis of light elements. Geostand Newsl 25:441–463. doi:10.1111/j.1751-908X.2001.tb00616.x

Groat LA et al (2002) Mineralogical and geochemical study of the Regal Ridge emerald showing, southeastern Yukon. Can Mineral 40:1313–1338. doi:10.2113/gscanmin.40.5.1313

Grundmann G (1983) Die Genese der regionalmetamorphen, metasomatisch-horizontgebundenen Beryll-Mineralisationen des Habachtals, Land Salzburg, Österreich. Dissertation TU Berlin D83: 207 p

Grundmann G (1989) Metamorphic evolution of the Habach formation—a review. Österr Mineral Gesell Mitt 82:75–88

Grundmann G (1991) Smaragd. Grünes Feuer unterm Eis. Extra Lapis, 1, Christian Weise Verlag, München, 96 p

Grundmann G, Morteani G (1982) Die Geologie des Smaragdvorkommens im Habachtal (Land Salzburg, Österreich). Arch Lagerstattenforschung Geologische Bundesanstalt Wien 2:71–107

Grundmann G, Morteani G (1989) Emerald mineralization during regional metamorphism: the Habachtal (Austria) and Leydsdorp (Transvaal, South Africa) deposits. Econ Geol 84:1835–1849

Hawthorne FC, Henry DJ (1999) Classification of the minerals of the tourmaline group. Eur J Mineral 11:201–215

Henry DJ, Dutrow BL (1996) Metamorphic tourmaline and its petrologic applications. Min Soc Am Rev Miner 33:503–558

Henry DJ, Guidotti CV (1985) Tourmaline as a petrogenetic indicator mineral: an example from the staurolite-grade metapelites of NW Maine. Am Mineral 70:1–15

Hoernes S, Friedrichsen H (1974) Oxygen isotope studies on metamorphic rocks of the western Hohe Tauern area (Austria). Schweiz Min Petr Mitt 54:769–788

Kasemann S, Erzinger J, Franz G (2000) Boron recycling in the continental crust of the central Andes from the Palaeozoic to Mesozoic, NW Argentina. Contrib Mineral Petrol 140:328–343. doi:10.1007/s004100000189

King RL, Kohn MJ, Eiler JM (2003) Constraints on the petrologic structure of the subduction zone slab-mantle interface from Franciscan Complex exotic ultramafic blocks. Geol Soc Am Bull 115:1097–1109. doi:10.1130/B25255.1

Marschall HR, Ludwig T, Altherr R, Kalt A, Tonarini S (2006) Syros metasomatic tourmaline: evidence for very high-δ^{11}B fluids in subduction zones. J Petrol 47:1915–1942. doi:10.1093/petrology/egl031

Melcher F, Meisel T, Puhl J, Koller F (2002) Petrogenesis and geotectonic settting of ultramafic rocks in the Eastern Alps: constraints from geochemistry. Lithos 65:69–112. doi:10.1016/S0024-4937(02)00161-5

Meyer C, Wunder B, Meixner A, Romer RL, Heinrich W (2008) Boron-isotope fractionation between tourmaline and fluid: an experimental re-investigation. Contrib Mineral Petrol 156:259–267. doi:10.1007/s00410-008-0285-1

Morteani G (1974) Petrology of the Tauern Window. Austrian Alps. Fortschritt Miner 52:195–220

Morteani G, Grundmann G (1977) The emerald porphyroblasts in the penninic rocks of the Tauern Window, Austrian Alps. N Jb Miner Mh 11:509–516

Nwe YY, Grundmann G (1990) Evolution of metamorphic fluids in shear zones: the record from the emeralds of Habachtal, Tauern Window, Austria. Lithos 25:281–304. doi:10.1016/0024-4937(90)90027-X

Okrusch M, Richter P, Guerkan A (1981) Geochemistry of blackwall sequences in the Habachtal emerald deposits, Hohe Tauern, Part 1: presentation of geochemical data. Tschermak Min Petr Mitt 29:9–31. doi:10.1007/BF01082812

Palmer MR, London D, Morgan GBVI, Babb HA (1992) Experimental determination of fractionation of 11B/10B between tourmaline and aqueous vapor. A temperature and pressure-dependent isotopic system. Chem Geol 101:123–129

Palmer MR, Swihart GH (1996) Boron isotope geochemistry: an overview. Min Soc Am Rev Miner 33:709–744

Phillips AH, Hess HH (1936) Metamorphic differentiation at contacts between serpentinite and siliceous country rocks. Am Mineral 21:333–362

Pouchou JL, Pichoir F (1984) An new model of quantitative X-ray microanalysis—part 1: application to the analysis of homogeneous samples. Rech Aerosp 3:13–38

Schmidt C, Thomas R, Heinrich W (2005) Boron speciation in aqueous fluids at 22 to 600°C and 0.1 MPa to 2 Gpa. Geochim Cosmochim Acta 69:275–281. doi:10.1016/j.gca.2004.06.018

Seifert AV, Zacez V, Vrana S, Pecina V, Zacharias J, Zwaan JC (2004) Emerald mineralization in the Kafubu Area, Zambia. Czech Geol Surv Bull Geosci 79:1–40

Tonarini S, Pennisi M, Adorni-Braccesi A, Dini A, Ferrara G, Gonfiantini R et al (2003) Intercomparison of Boron isotope and concentration measurements. Part I: selection, preparation and homogeneity tests of the intercomparison materials. Geostand Newsl 27:21–39. doi:10.1111/j.1751-908X.2003.tb00710.x

Trumbull RB, Krienitz M-S, Gottesmann B, Wiedenbeck M (2008) Chemical and boron-isotope variations in tourmalines from an S-type granite and its source rocks: the Erongo granite and tourmalinites in the Damara Belt, Namibia. Contrib Mineral Petrol 155:1–18. doi:10.1007/s00410-007-0227-3

Williams LB, Hervig RL, Holloway JR, Hutcheon I (2001) Boron isotope geochemistry during diagenesis. Part 1. Experimental determination of fractionation during illitization of smectite. Geochim Cosmochim Acta 65:1769–1782. doi:10.1016/S0016-7037(01)00557-9

Wunder B, Meixner A, Romer RL, Wirth R, Heinrich W (2005) The geochemical cycle of boron: constraints from boron isotope partitioning experiments between mica and fluid. Lithos 84:206–216. doi:10.1016/j.lithos.2005.02.003

van Hinsberg VJ, Schumacher JC, Kearns S, Mason PRD, Franz G (2006) Hourglass sector zoning in tourmaline and resultant major and trace element fractionation. Am Mineral 91:717–728

van Hinsberg VJ, Marschall HR (2007) Boron isotope and light element sector zoning in tourmaline: implications for the formation of B-isotope signatures. Chem Geol 238:141–148

van Hinsberg VJ, Schumacher JC (2007) Intersector chemical partitioning in tourmaline: a potentially powerful single crystal thermometer. Contrib Mineral Petrol 153:289–301